International Journal of Distributed Sensor Networks

*International Journal of Distributed Sensor Networks*
2020, Vol. 16(6)

DOI: 10.1177/1550147720912950
journals.sagepub.com/home/dsn
SAGE

# MIMO-OFDM/OCDM low-complexity equalization under a doubly dispersive channel in wireless sensor networks

**Ahmad AA Solyman[1], Hani Attar[2], Mohammad R Khosravi[3] and Baki Koyuncu[1]**

## Abstract

In this article, three novel systems for wireless sensor networks based on Alamouti decoding were investigated and then compared, which are Alamouti space–time block coding multiple-input single-output/multiple-input multiple-output multicarrier modulation (MCM) system, extended orthogonal space–time block coding multiple-input single-output MCM system, and multiple-input multiple-output system. Moreover, the proposed work is applied over multiple-input multiple-output systems rather than the conventional single-antenna orthogonal chirp division multiplexing systems, based on the discrete fractional cosine transform orthogonal chirp division multiplexing system to mitigate the effect of frequency-selective and time-varying channels, using low-complexity equalizers, specifically by ignoring the intercarrier interference coming from faraway subcarriers and using the LSMR iteration algorithm to decrease the equalization complexity, mainly with long orthogonal chirp division multiplexing symbols, such as the TV symbols. The block diagrams for the proposed systems are provided to simplify the theoretical analysis by making it easier to follow. Simulation results confirm that the proposed multiple-input multiple-output and multiple-input single-output orthogonal chirp division multiplexing systems outperform the conventional multiple-input multiple-output and multiple-input single-output orthogonal frequency division multiplexing systems. Finally, the results show that orthogonal chirp division multiplexing exhibited a better channel energy behavior than classical orthogonal frequency division multiplexing, thus improving the system performance and allowing the system to decrease the equalization complexity.

## Keywords

Orthogonal chirp division multiplexing, multiple-input multiple-output, orthogonal frequency division multiplexing, wireless sensor networks, doubly dispersive channel, intercarrier interference

Date received: 2 November 2019; accepted: 20 February 2020

Handling Editor: Ashish Kr Luhach

## Introduction

Previously, the single-input single-output (SISO) orthogonal frequency division multiplexing (OFDM) and orthogonal chirp division multiplexing (OCDM) systems based on discrete fractional Fourier transform (DFrFT) and discrete fractional cosine transform (DFrCT) were investigated carefully under the doubly dispersive channel scenario in previous studies.[1–5] It was found that OCDM systems outperform the

[1]Department of Electrical and Electronics Engineering, Istanbul Gelisim University, Istanbul, Turkey
[2]Department of Energy Engineering, Zarqa University, Zarqa, Jordan
[3]Department of Electrical and Electronic Engineering, Shiraz University of Technology, Shiraz, Iran

**Corresponding author:**
Hani Attar, Department of Energy Engineering, Zarqa University, P.O. Box 132222, Zarqa 13132, Jordan.
Email: hattar@zu.edu.jo

OFDM systems that the OCDM systems can cope perfectly with the doubly dispersive channel variations. Roughly speaking, the OCDM subchannel carrier frequencies are time-varying and ideally decompose the frequency distortion of the channel perfectly at any instant in time as the OCDM chirp bases match the essential time-varying characteristics of the doubly dispersive channel.[6]

Currently, there is a great demand on higher data throughput with a limited bandwidth that is facilitated using multiple-input multiple-output (MIMO) systems. MIMO is one of the several forms of smart antenna technologies which improve the communication performance using more than one antenna at the transmitter and the receiver. A popular approach in MIMO systems is to combine it with multicarrier methods such as OFDM to improve the overall system performance which is known as MIMO-OFDM.

A primary example of MIMO-OFDM is the multiple-input single-output (MISO) Alamouti space–time block coding (STBC) and the MISO extended orthogonal space–time block coding (EO-STBC) combined with the OFDM system to achieve locative and multipath variety gains and to decrease the intercarrier interference (ICI) error level. Nevertheless, under high-speed movement of the transmitter, receiver, or both; applying the Alamouti STBC or the EO-STBC over nearby OFDM symbols is regarded as not successful due to the major channel time disparity.

In this article, three novel systems are introduced which are Alamouti STBC MISO multicarrier modulation (MCM) system, EO-STBC MISO MCM system, and MIMO system, based on the OCDM MCM systems which are shown to improve these systems' performance under the doubly dispersive channel scenario. In addition, MIMO systems are investigated in this article, together with the Alamouti STBC MISO system, the EO-STBC MISO system, and the MIMO system accompanied with the OCDM MCM systems. The explanation of the key implementation of the transceiver is provided to make the full picture of the suggested work clearer. The system's equalization problem is stated in this work and a comparison between complicated equalizers and low-complexity equalizers is made.

## MIMO systems

The earliest ideas in MIMO belong to the work by Kaye and George[7] and Brandenburg and Wyner.[8] MIMO is one of the most important technologies in wireless communications, as it compromises an increase in the data throughput and the connection range, without requiring an extra bandwidth or a transmission power. MIMO does so by splitting the total power conducted over the system antennas to obtain the gain array, thus improving the spectrum efficiency (more bits per second per hertz of bandwidth), and/or to obtain diversity gain which enhances the link consistency by reducing the fading effect. These properties increased the interest in MIMO to become an important part in the recent wireless communication standards, such as IEEE 802.11 b/g/n Wi-Fi, WiMAX, and 5G.

There are several particular cases of MIMO such as SISO/single-input multiple-output (SIMO)/MISO where SISO is the standard radio arrangement, that is, the transmitter and the receiver each have only one antenna, taking into consideration the fact that the MISO is regarded as a special case when the transmitter has more than one antennas and the receiver has a single antenna, while SIMO is regarded as the special case when the transmitter has one antenna and the receiver has several antennas.

Siavash M Alamouti[9] proposed a simple MISO system using two transmitting antennas and one receiving antenna; this algorithm is called STBC providing a full diversity order. More details about the Alamouti scheme are presented in the next section of this article.

Some innovative diversity systems such as EO-STBC, where degree one and extreme diversity order are accomplished concurrently, regardless of the process with four transmitting antennas, because of the use of extra beam steering that is established on the feedback of channel state information (CSI).[10,11]

Alamouti STBC and the EO-STBC systems have been produced in the context of narrow-band static channels. In frequency fading channel conditions, an arrangement with multicarrier systems such as OFDM[12] is used, in order to operate narrow-band Alamouti STBC and EO-STBC systems in separate subcarriers, which are clear of intersymbol interference (ISI) and ICI. In the circumstance of narrow-band time-varying systems; the scheme degradation is minimal on condition that the channel disparity over one Alamouti STBC or EO-STBC symbol can be defined as a minor variation. Nevertheless, if a time-varying channel exhibits additional delay spread, then the classical use of multicarrier methods leads to considerably longer symbol periods, which will require the introduction of various equalisation approaches in the frequency domain such as zero-forcing (ZF) and minimum mean square error (MMSE) schemes,[13] or other receivers are to be applied for the individual subcarriers, including the ZF, decision-feedback (DF), and joint maximum-likelihood (JML) detectors,[1,2] however, the neglected ICI introduces an error floor on the bit error rate (BER) performance as loss of orthogonality is increased.

In previous studies,[3,14–16] the loss of OFDM orthogonality in doubly dispersive channels was studied and multicarrier schemes based on DFrFT and DFrCT were developed that the DFrFT and the DFrCT-OCDM schemes granted better performance in the doubly dispersive channel scenario. Therefore, a novel combination of the DFrFT and DFrCT-OCDM systems with Alamouti and EO-STBC is proposed in the following sections, together with investigating the combination of conventional and low-cost equalization approaches.

## Fractional Fourier transform and fractional cosine transform

The fractional Fourier transform (FrFT) is a generalization of the Fourier transform (FT) and can be viewed as the fractional power of the FT operator. In the time–frequency plane, the original signal in the time domain represented by $f(t)$ and $F_\alpha(u)$ is the counterpart in the $\alpha$th-order}} fractional domain.

The transformation kernel of the continuous FrFT is defined as[17]

$$K_\alpha(t,u) = A_\alpha e^{j\pi\left(t^2+u^2\right)\cot\alpha - j2\pi tu\csc\alpha} \tag{1}$$

where $\alpha$ is the rotation angle for the transformation process and

$$A_\alpha = \frac{e^{\{-j\pi sign[\sin\alpha]/4 + j\alpha/2\}}}{\sqrt{|\sin\alpha|}} \tag{2}$$

The forward FrFT is defined as

$$f_\alpha\{x(t)\}(u) = X_\alpha(u) = \int_{-\infty}^{\infty} x(t)K_\alpha(t,u)dt \tag{3}$$

$$x(t) = \int_{-\infty}^{\infty} X_\alpha(u)K_{-\alpha}(t,u)du \tag{4}$$

The domains of the signal for $0<|\alpha|<\pi$ define the fractional Fourier domains. Substituting with $\alpha = \pi/2$ in equation (3) and equation (4) gives the well-known Fourier transform.

By extension, fractional cosine transform may be considered as a generalization of the discrete cosine transform (DCT), the $\alpha$th-order fractional cosine transform is given by[18,19]

$$F_\alpha^c(u) = A_\alpha e^{j\left(\frac{u^2}{2}\right)\cot\alpha} \int_{-\infty}^{\infty} \cos(\csc\alpha \cdot ut) e^{j\left(\frac{t^2}{2}\right)\cot\alpha} f(t)dt \tag{5}$$

where the angle between the fractional order axis $u$ and the time axis $t$ is $\alpha = -\pi/2$ to $\pi/2$, and $A_\alpha = \sqrt{(1-j\cot\alpha)/2\pi}$.

Various definitions of the DFrCT differ in accuracy and complexity and may be derived using extensions from the FrFT by sampling the real/imaginary parts of the FrFT kernel or directly from the DCT itself.[20] The definition of DFrCT in Soo-Chang and Min-Hung[19] is used in our work. It has minimal complexity and a simple inverse transform. In the following, we will denote the DFrCT as $F_\alpha = F_\alpha^c$. In Solyman et al.,[16] the DFrCT uses the discrete Fourier transform (DFT) Hermitian eigenvector decomposition and the DCT transform kernel.

The vector notation for the DFrCT is given by

$$X = \begin{bmatrix} X_\alpha(0) \\ X_\alpha(1) \\ \vdots \\ X_\alpha(N-1) \end{bmatrix} = F_\alpha \begin{bmatrix} x(0) \\ x(1) \\ \vdots \\ x(N-1) \end{bmatrix} = F_\alpha \cdot x \tag{6}$$

where $F_\alpha$ is the unitary $N \times N$ DFrCT matrix, $N$ is the number of samples, and $\alpha$ indicates the rotation angle of transform in the time–frequency plane. Note that, when $\alpha = \pi/2$, the DFrCT will become the conventional DCT and when $\alpha = 0$, $F_\alpha$ is an identity matrix.[19] Similarly, the inverse discrete fractional cosine transform (IDFrCT) can be written as

$$x = F_{-\alpha}.X \tag{7}$$

where $F_{-\alpha} = F_\alpha^H$ and $(\cdot)^H$ denotes the complex conjugate transpose operation.

### DFrCT complexity

Implementing the FrFT for a given signal requires two chirp multiplications and one DFT,[20] since an efficient DFT requires approximately $(P/3)\log_2 P$ complex multiplications (using the split-radix algorithm) where $P$ is the total number of sampling points. Therefore, a total of approximately $2P + (P/3)\log_2 P$ complex multiplications are required to implement the FrFT. Because each complex number multiplication requires a minimum of three real number multiplications, the number of real number multiplications required for the FrFT is

$$6P + P \cdot \log_2 P \tag{8}$$

Using similar arguments and by computing the DFrCT from the first-type DCT kernel,[20] the DFrCT requires

$$2P + (P/2) \cdot \log_2(P/2) \tag{9}$$

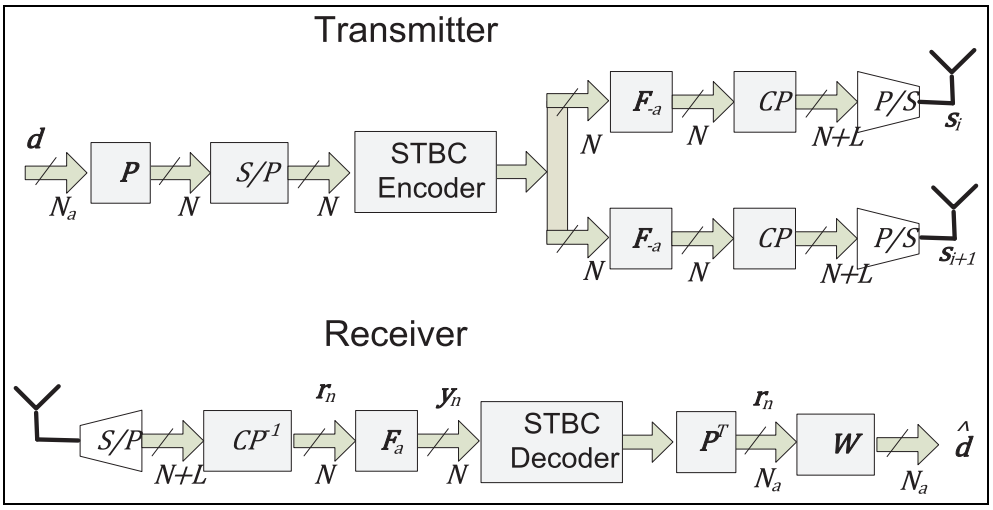


**Figure 1.** The Alamouti coded OCDM system.

Consequently, the complexity of the FrCT is approximately half that of the FrFT.

## OCDM Alamouti MISO STBC system

The point-to-point OCDM multicarrier system based on Alamouti's[9] scheme presented in Paige and Saunders[21] is adapted in this article, and the scheme is implemented using two antennas on the transmitter side and one antenna on the receiver side as shown in Figure 1. It is assumed that the same transmission system of the SISO-OCDM system is used, except that every two consecutive OCDM symbols are considered as an Alamouti code word. Assume that $\boldsymbol{s}_1$ and $\boldsymbol{s}_2$ are the two successive OCDM symbols, where the vector $\boldsymbol{s}_i = [s_0 \quad s_1 \quad \ldots \quad s_N]^T$ is given by

$$\boldsymbol{s}_i = \boldsymbol{F}_{-\alpha}\boldsymbol{P}\boldsymbol{d}_i \tag{10}$$

where $\boldsymbol{F}_{-\alpha}$ can be the inverse discrete fractional Fourier transform (IDFrFT) or IDFrCT transformation matrix and $\boldsymbol{P}$ is defined as

$$\boldsymbol{P} = \left[0_{N_a \times (N-N_a)/2} \boldsymbol{I}_{N_a} 0_{N_a \times (N-N_a)/2}\right] \tag{11}$$

where $0_{X \times Y}$ is an $X \times Y$ zero matrix and $\boldsymbol{I}_X$ is an $X \times X$ unit matrix.

$\boldsymbol{s}_1$ and $\boldsymbol{s}_2$ transmitted throughout the first OCDM symbol period, then $-\boldsymbol{s}_2^*$ and $\boldsymbol{s}_1^*$ transmitted throughout the second OCDM symbol period from antennas 1 and 2 correspondingly. On the receiver side, we start by eliminating the cyclic prefix (CP); the received signals in two consecutive OCDM symbol periods can be written as

$$\boldsymbol{r}_1 = \boldsymbol{H}_{1,1}\boldsymbol{s}_1 + \boldsymbol{H}_{2,1}\boldsymbol{s}_2 + \boldsymbol{z}_1 \tag{12}$$

$$\boldsymbol{r}_2 = -\boldsymbol{H}_{1,2}\boldsymbol{s}_2^* + \boldsymbol{H}_{2,2}\boldsymbol{s}_1^* + \boldsymbol{z}_2 \tag{13}$$

where $\boldsymbol{r}_i$ is the received $N$ vector in the $i$th symbol period, $\boldsymbol{H}_{i,j}$ is the time-domain channel matrix between the transmitting antenna $i$ and the receiving antenna in symbol time $j$, and $\boldsymbol{z}$ is the zero-mean complex Gaussian random noise.

The DFrCT demodulates the received signal; accordingly, the two successive demodulated received signals are given by

$$\boldsymbol{y}_1 = \boldsymbol{F}_\alpha \boldsymbol{r}_1 \tag{14}$$

$$\boldsymbol{y}_2 = \boldsymbol{F}_\alpha \boldsymbol{r}_2 \tag{15}$$

Combining $\boldsymbol{y}_1$ and $\boldsymbol{y}_2^*$ in the same equation, we obtain

$$\begin{bmatrix} \boldsymbol{y}_1 \\ \boldsymbol{y}_2^* \end{bmatrix} = \begin{bmatrix} \tilde{\boldsymbol{H}}_{1,1} & \tilde{\boldsymbol{H}}_{2,1} \\ \tilde{\boldsymbol{H}}_{2,2}^* & -\tilde{\boldsymbol{H}}_{1,2}^* \end{bmatrix} \begin{bmatrix} \boldsymbol{P}.\boldsymbol{d}_1 \\ \boldsymbol{P}.\boldsymbol{d}_2 \end{bmatrix} + \begin{bmatrix} \tilde{\boldsymbol{z}}_1 \\ \tilde{\boldsymbol{z}}_2^* \end{bmatrix} \tag{16}$$

where $\tilde{z}_i = F_\alpha z_i$ is the noise vector in the frequency domain and $\tilde{H}_{i,j} = F_\alpha H_{i,j} F_\alpha^H$ is the system matrix; in the case where the channel is changing over time, $\tilde{H}_{i,j}$ is almost banded matrix with the greatest significant components around the main diagonals as shown in Figure 2, which permits the use of reduced-complexity equalizers as recommended in previous studies.[4,5,22,23] The fractional domain channel matrix $\tilde{H}_{i,j}$ can be approximated by its banded form using the banded matrix which is written as

$$\boldsymbol{B}_{i,j} = \boldsymbol{M} \odot \tilde{\boldsymbol{H}}_{i,j} \tag{17}$$

where $\boldsymbol{M}(m,n)$ is a Toeplitz binary matrix given by

$$\boldsymbol{M}(m,n) = \begin{cases} 1, & 0 \leqslant |m-n| \leqslant Q \\ 0, & Q < |m-n| < N_a \end{cases} \tag{18}$$

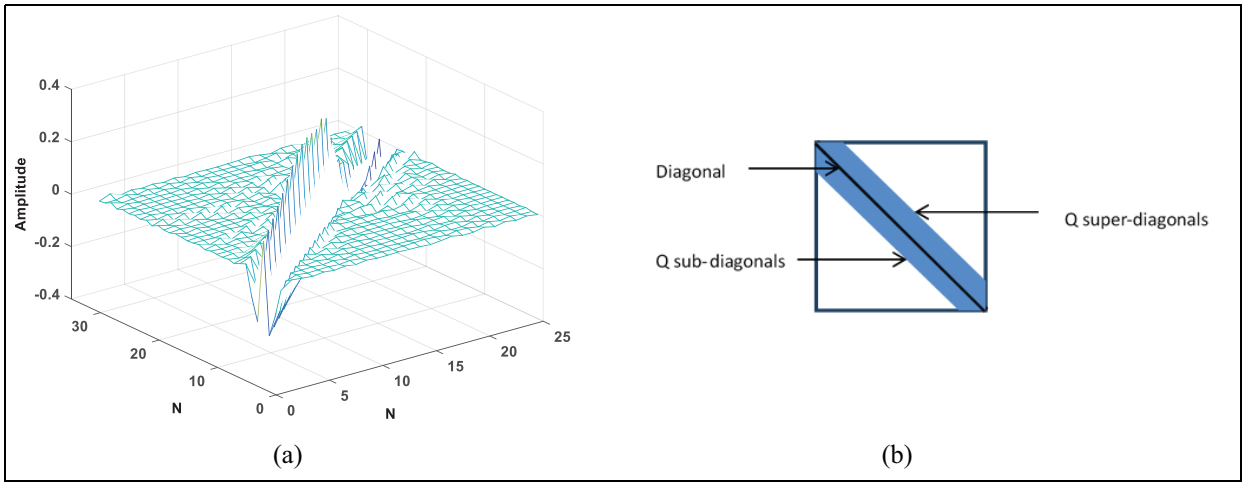


**Figure 2.** (a) Fractional domain doubly dispersive channel matrix with $N = 35$ and (b) the desired structure for the band matrix $B$.

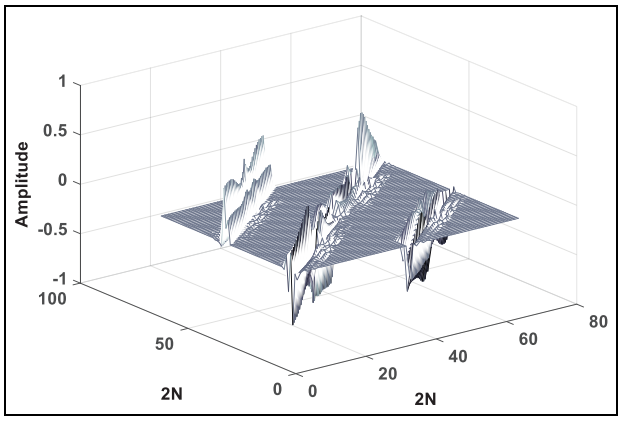


**Figure 3.** Fractional domain doubly dispersive banded channel matrix $B$ with $N = 35$.

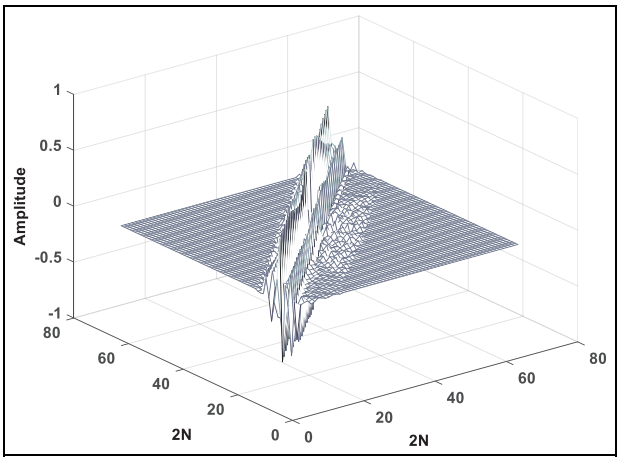


**Figure 4.** Fractional domain doubly dispersive banded channel matrix after permutation $\boldsymbol{B}_{\mathcal{P}}$ with $N = 35$.

In equation (17), $Q$ is used to control how many sub- and super-diagonals of $\tilde{\boldsymbol{H}}_{i,j}$ elements should be constituted to provide a decent approximation of the banded fractional domain channel matrix. The $Q$ modification simplifies a compromise among the equalizer complexity and the system efficiency. As a result, equation (16) can be written as

$$\boldsymbol{Y} = \boldsymbol{B}\boldsymbol{d} + \boldsymbol{z} \tag{19}$$

where $\boldsymbol{B}$ is a $2 \times 2$ block matrix of $\boldsymbol{B}_{i,j}(N \times N)$ banded matrices as shown in Figure 3. $\boldsymbol{B}$ can be converted into a $2N \times 2N$ banded matrix using permutation matrix $\mathcal{P}$, which is a $2N \times 2N$ matrix with 1's at locations $\{(i+1, (i)_{\text{div2}} + 1 + N(i)_{\text{mod2}})\}_{i=0}^{2N-1}$ and 0's elsewhere.[24] Multiplying equation (19) by $\mathcal{P}$, we obtain

$$\begin{aligned} \boldsymbol{Y}_{\mathcal{P}} &= \mathcal{P}\boldsymbol{Y} = \mathcal{P}\boldsymbol{B}\mathcal{P}^{T}\mathcal{P}\boldsymbol{d} + \mathcal{P}\boldsymbol{z} \\ &= \boldsymbol{B}_{\mathcal{P}}\boldsymbol{d}_{\mathcal{P}} + \boldsymbol{z}_{\mathcal{P}} \end{aligned} \tag{20}$$

where $\boldsymbol{B}_{\mathcal{P}}$ is the permuted banded fractional domain channel matrix as shown in Figure 4, and $\boldsymbol{Y}_{\mathcal{P}}$ and $\boldsymbol{d}_{\mathcal{P}}$ are the permuted transmitted and received signals, respectively. Now $\boldsymbol{d}_{\mathcal{P}}$ is the grouped collected data of different transmitting antennas from the same subcarriers and $\boldsymbol{Y}_{\mathcal{P}}$ is the grouped received data from the same subcarriers in two consecutive OCDM symbol periods.

## *Low-complexity MMSE equalizer*

The low-complexity MMSE equalizers proposed for OFDM in Solyman et al.[3,16] will be extended to the MISO Alamouti coding scheme in this section.

Ideal knowledge of the channel matrix $\boldsymbol{B}_{\mathcal{P}}$ is supposed, and there is no guard subcarriers used by the equalizer. Also, it is assumed that $E\{\boldsymbol{d}\} = E\{\boldsymbol{z}\} = 0$, $E\{\boldsymbol{d}\boldsymbol{d}^{H}\} = \boldsymbol{I}$, $E\{\boldsymbol{d}\boldsymbol{z}^{H}\} = 0$, $E\{\boldsymbol{z}\boldsymbol{z}^{H}\} = \sigma^{2}\boldsymbol{I}$. Because of

the inversion of the channel matrix which needs $\mathcal{O}(N_A^3)$ complex operations, the MMSE equalizer is complex, especially for high values of $N_A$. Such assumptions are accepted and the generality of the work is not lost.

The MMSE equalizer $\boldsymbol{W}_{MMSE}$ is given by

$$\boldsymbol{W}_{MMSE} = \left(\boldsymbol{B}_{\mathcal{P}}\boldsymbol{B}_{\mathcal{P}}^H + \gamma^{-1}\boldsymbol{I}_{N_A}\right)^{-1}\boldsymbol{B}_{\mathcal{P}}^H \tag{21}$$

The estimated data are given by

$$\hat{\boldsymbol{d}}_{MMSE} = \boldsymbol{W}_{MMSE}\boldsymbol{Y}_{\mathcal{P}} \tag{22}$$

where $\hat{\boldsymbol{d}}_{MMSE}$ is the permuted version of $\hat{\boldsymbol{d}}$ which can be reconstructed by

$$\hat{\boldsymbol{d}} = \mathcal{P}^T\hat{\boldsymbol{d}}_{MMSE} \tag{23}$$

The overall complexity for obtaining $\hat{\boldsymbol{d}}_n$ is $(8Q^2 + 22Q + 4)N_a$ complex operations.[5] The parameter $Q$ choice is a trade-off between performance and complexity. This implies that choosing a larger $Q$ yields a smaller approximation error and therefore a performance improvement. However, the resulting complexity increases due to the increase in the bandwidth of $\boldsymbol{B}$.

Applying $LDL^{H}$[25] matrix factorization in computing MMSE solutions in equation (49) will reduce the number of complex processes related to standard matrix inversion methods, such as Gaussian elimination to $\mathcal{O}(8Q^2 + 22Q + 4)2N_a$ complex processes.

Using the same formulation with the iterative MMSE equalization that applies the least-square minimal residual method iterative algorithm (LSMR) algorithm as in Solyman et al.[3] results in reducing the equalizer complexity to $\mathcal{O}(N_A(Q+1)\boldsymbol{I})$ complex operations in total for the banded matrix case, where $\boldsymbol{I}$ is the number of iterations.

The $LDL^H$ factorization of the Hermitian band matrix $\boldsymbol{B}_n\boldsymbol{B}_n^H + \gamma^{-1}\boldsymbol{I}_{N_a} = \boldsymbol{L}\boldsymbol{D}\boldsymbol{L}^H$ is numerically straight forward,[25] and leads to

$$\hat{\boldsymbol{d}}_n = \boldsymbol{B}_n^H\left(\boldsymbol{L}\boldsymbol{D}\boldsymbol{L}^H\right)^{-1}\tilde{\boldsymbol{r}}_n = \boldsymbol{B}_n^H\boldsymbol{x}_n \tag{24}$$

Instead of calculating the inverse in equation (24), the system

$$\left(\boldsymbol{L}\boldsymbol{D}\boldsymbol{L}^H\right)^{-1}\tilde{\boldsymbol{r}}_n = \boldsymbol{x}_n \tag{25}$$

$$\tilde{\boldsymbol{r}}_n = \left(\boldsymbol{L}\boldsymbol{D}\boldsymbol{L}^H\right)\boldsymbol{x}_n \tag{26}$$

$$\tilde{\boldsymbol{r}}_n = \boldsymbol{L}\underbrace{\boldsymbol{D}\overbrace{\boldsymbol{L}^H\boldsymbol{x}_n}^{\boldsymbol{x}_{1,n}}}_{\boldsymbol{x}_{2,n}} \tag{27}$$

is solved by forward substitution to obtain $\boldsymbol{x}_{2,n}$ via the lower left triangular matrix $\boldsymbol{L}$ and a rescaling by the diagonal matrix $\boldsymbol{D}^{-1}$ to calculate $\boldsymbol{x}_{1,n}$. Finally, backsubstitution with the upper right triangular $\boldsymbol{L}^H$ yields $\boldsymbol{x}_n$, which can be inserted into equation (24) in order to determine $\hat{\boldsymbol{d}}_n$.

The overall complexity for obtaining $\hat{\boldsymbol{d}}_n$ is $(8Q^2 + 22Q + 4)N_a$ complex operations.[5] The parameter $Q$ choice is a trade-off between performance and complexity. This implies that choosing a larger $Q$ yields a smaller approximation error and therefore a performance improvement. However, the resulting complexity increases due to the higher bandwidth of $\boldsymbol{B}$, and vice versa.

## Low-complexity LSMR equalization

MMSE equalizer complexity comes from the matrix inversion in equation (21), and solving this matrix inversion iteratively is one of the clever ideas to reduce the MMSE equalizer complexity. In previous studies,[26–29] the authors use the iterative LSQR (An algorithm for sparse linear equations and sparse least squares) algorithm,[21] which exhibits excellent performance in solving the channel matrix inversion problem (typically ill-conditioned matrix) by early termination of the iterations at low complexity as the complexity order per iteration is $\mathcal{O}(N_aN_h)$ operations, where $N_h$ is the maximum delay of the channel. Thus, the method is mostly smart when the channel's maximum delay is not too large. Recently, a new iterative algorithm called LSMR was proposed in Fong and Saunders.[30]

LSMR is an iterative algorithm for solving linear systems $\boldsymbol{A}\boldsymbol{x} = \boldsymbol{b}$, least-squares (LS) problems $\min \| \boldsymbol{A}\boldsymbol{x} - \boldsymbol{b}\|_2$, and regularized least squares (RLS) $\min\left\|\begin{pmatrix}\boldsymbol{A}\\ \lambda\boldsymbol{I}\end{pmatrix}\boldsymbol{x} - \begin{pmatrix}\boldsymbol{b}\\ 0\end{pmatrix}\right\|_2$ with $A$ being sparse or a fast linear operator.[30] LSMR is based on the Golub–Kahan bidiagonalization process and analytically equivalent to the minimal residual method (MINRES)[31] applied to the normal equation $\boldsymbol{A}^T\boldsymbol{A}\boldsymbol{x} = \boldsymbol{A}^T\boldsymbol{b}$. LSMR is similar in style to the well-known method LSQR in being based on the Golub–Kahan bidiagonalization of $\boldsymbol{A}$.

LSQR is equivalent to the conjugate gradient (CG) method applied to the normal equation $(\boldsymbol{A}^T\boldsymbol{A} + \lambda^2\boldsymbol{I})\boldsymbol{x} = \boldsymbol{A}^T\boldsymbol{b}$. It has the property of reducing $\| \boldsymbol{r}_k \|$ monotonically, where $\boldsymbol{r}_k = \boldsymbol{b} - \boldsymbol{A}\boldsymbol{x}_k$ is the residual for the approximate solution $\boldsymbol{x}_k$. On the other hand, LSMR has the property of reducing both $\| \boldsymbol{r}_k \|$ and $\| \boldsymbol{A}^T\boldsymbol{r}_k \|$ monotonically. Although LSQR and LSMR ultimately converge to similar points, LSMR converges faster with fewer iterations. LSMR can solve the inversion matrix problem in the MMSE equalizer more effectively with less computational cost due to its faster conversion to the solution.

### LSMR algorithm

The LSMR algorithm aims to approximately solve the linear equation given by

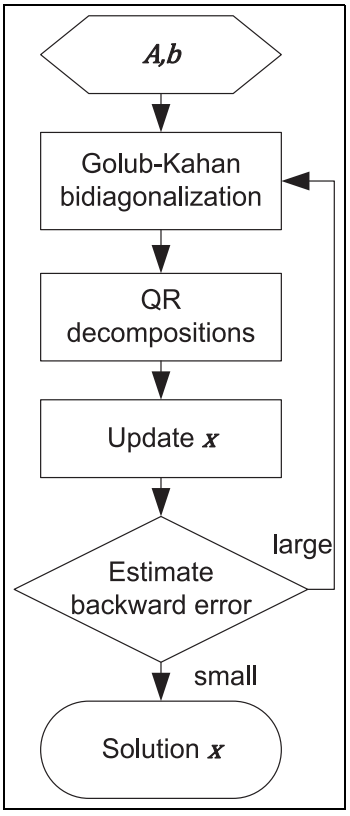


**Figure 5.** LSMR algorithm flowchart.

$$\boldsymbol{A^T A x} = \boldsymbol{A^T b} \tag{28}$$

$$\min \| \boldsymbol{Ax} - \boldsymbol{b} \|_2 \tag{29}$$

and the RLS given by

$$(\boldsymbol{A^T A} + \lambda^2 \boldsymbol{I})\boldsymbol{x} = \boldsymbol{A^T b} \tag{30}$$

$$\min \left\| \begin{pmatrix} \boldsymbol{A} \\ \lambda \end{pmatrix} \boldsymbol{x} - \begin{pmatrix} \boldsymbol{b} \\ \boldsymbol{0} \end{pmatrix} \right\|_2 \tag{31}$$

with $\boldsymbol{A}$ being sparse or a fast linear operator. The flowchart of the LSMR algorithm is shown in Figure 5.

For simplicity, considering equation (28) given $\boldsymbol{A}(m \times n)$ and $\boldsymbol{b}(m \times 1)$ starting from Golub–Kahan bidiagonalization,[32] the direct bidiagonalization is given by

$$\boldsymbol{U}^T(\boldsymbol{bA}) \begin{pmatrix} 1 & \times \\ \times & \boldsymbol{V} \end{pmatrix} = \begin{pmatrix} \times & \times & 0 & 0 \\ 0 & \times & \times & 0 \\ 0 & 0 & \times & \times \\ 0 & 0 & 0 & \times \end{pmatrix} \tag{32}$$

$$\Rightarrow (\boldsymbol{b} \quad \boldsymbol{AV}) = \boldsymbol{U}(\boldsymbol{\beta}_1 \boldsymbol{e}_1 \quad \boldsymbol{B})$$

Using iterative bidiagonalization Bidiag$(A, b)$, we obtain

$$\boldsymbol{b} = \boldsymbol{U}_{k+1}(\boldsymbol{\beta}_1 \boldsymbol{e}_1) \tag{33}$$

$$\boldsymbol{A V}_k = \boldsymbol{U}_{k+1} \boldsymbol{B}_k \tag{34}$$

$$\boldsymbol{A}^T \boldsymbol{U}_k = \boldsymbol{V}_k \boldsymbol{B}_k^T \begin{pmatrix} \boldsymbol{I}_k \\ 0 \end{pmatrix} \tag{35}$$

where

$$\boldsymbol{B}_k = \begin{pmatrix} \boldsymbol{\alpha}_1 & 0 & 0 & 0 \\ \boldsymbol{\beta}_1 & \boldsymbol{\alpha}_2 & 0 & 0 \\ 0 & \ddots & \ddots & 0 \\ 0 & 0 & \boldsymbol{\beta}_k & \boldsymbol{\alpha}_k \\ 0 & 0 & 0 & \boldsymbol{\beta}_{k+1} \end{pmatrix} \tag{36}$$

$$\text{and} \quad \begin{matrix} \boldsymbol{U}_k = (\boldsymbol{u}_1 & \ldots & \boldsymbol{u}_k) \\ \boldsymbol{V}_k = (\boldsymbol{v}_1 & \ldots & \boldsymbol{v}_k) \end{matrix}$$

with $\boldsymbol{V}_k$ spanning the Krylov subspace

$$\begin{aligned} &\text{span}\{v_1, \ldots, v_k\} = \text{span} \\ &\quad \left\{ \boldsymbol{A}^T \boldsymbol{b}, (\boldsymbol{A}^T \boldsymbol{A}) \boldsymbol{A}^T \boldsymbol{b}, \ldots, (\boldsymbol{A}^T \boldsymbol{A})^{k-1} \boldsymbol{A}^T \boldsymbol{b} \right\} \end{aligned} \tag{37}$$

Define $\boldsymbol{x}_k = \boldsymbol{V}_k \boldsymbol{y}_k$, sub-problem to solve

$$\min_{y_k} \| \boldsymbol{A}^T \boldsymbol{r}_k \| = \min_{y_k} \left\| \bar{\boldsymbol{\beta}}_1 \boldsymbol{e}_1 - \begin{pmatrix} \boldsymbol{B}_k^T \boldsymbol{B}_k \\ \bar{\boldsymbol{\beta}}_{k+1} \boldsymbol{e}_k^T \end{pmatrix} \right\| \tag{38}$$

where $\boldsymbol{r}_k = \boldsymbol{b} - \boldsymbol{A x}_k$ and $\bar{\boldsymbol{\beta}}_k = \boldsymbol{\alpha}_k \boldsymbol{\beta}_k$.

### *LSMR complexity*

The storage requirement and computational complexity can be compared for LSMR and LSQR on $\boldsymbol{Ax} \approx \boldsymbol{b}$ and MINRES on the normal equation $\boldsymbol{A^T A x} = \boldsymbol{A^T b}$. The vector storage (excluding storage for $\boldsymbol{A}$ and $\boldsymbol{b}$) is listed in Table 1. Recall that $\boldsymbol{A}$ is $(m \times n)$ and for LS systems $m$ may be considerably larger than $n$. $\boldsymbol{Av}$ denotes the working storage for the matrix–vector products, and $\boldsymbol{h}_k$ and $\bar{\boldsymbol{h}}_k$ are the scalar multiples of $\boldsymbol{w}_k$ and $\bar{\boldsymbol{w}}_k$, respectively. Work represents the number of floating-point multiplications required for each iteration. From Table 1, it can be seen that the complexity of the LSMR is slightly more than that of the LSQR.

## STBC scheme based on OCDM

EO-STBC is an MISO space–time coder system based on four antennas on the transmitter side and one antenna on the receiver side. It is a diversity scheme that can accomplish both full diversity gain and full rate via an additional feedback link from the receiver to the transmitter, to update the phase rotations applied in the transmitter; accordingly, both full diversity and array gain are ensured.[15,33]

**Table 1.** Storage and computational requirements for various LS methods.

| | Storage | | Work | |
|---|---|---|---|---|
| | *m* | *n* | *m* | *n* |
| LSMR | $\boldsymbol{Av}, \boldsymbol{u}$ | $\boldsymbol{x}, \boldsymbol{v}, \boldsymbol{h}, \bar{\boldsymbol{h}}$ | 3 | 6 |
| LSQR | $\boldsymbol{Av}, \boldsymbol{u}$ | $\boldsymbol{x}, \boldsymbol{v}, \boldsymbol{w}$ | 3 | 5 |
| MINRES on $\boldsymbol{A}^T\boldsymbol{Ax} = \boldsymbol{A}^T\boldsymbol{b}$ | $\boldsymbol{Av}$ | $\boldsymbol{x}, \boldsymbol{v}_1, \boldsymbol{v}_2, \boldsymbol{w}_1, \boldsymbol{w}_2, \boldsymbol{w}_3$ | | 8 |

LS: least-squares.

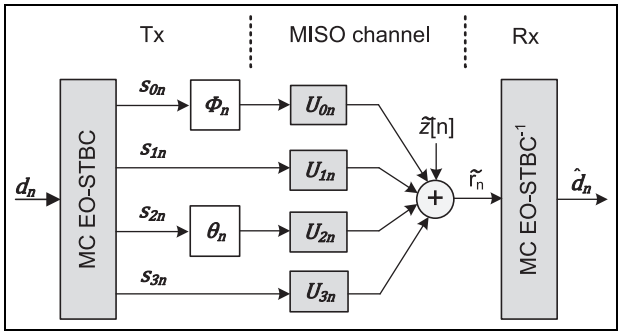


**Figure 6.** EO-STBC in a multicarrier configuration.

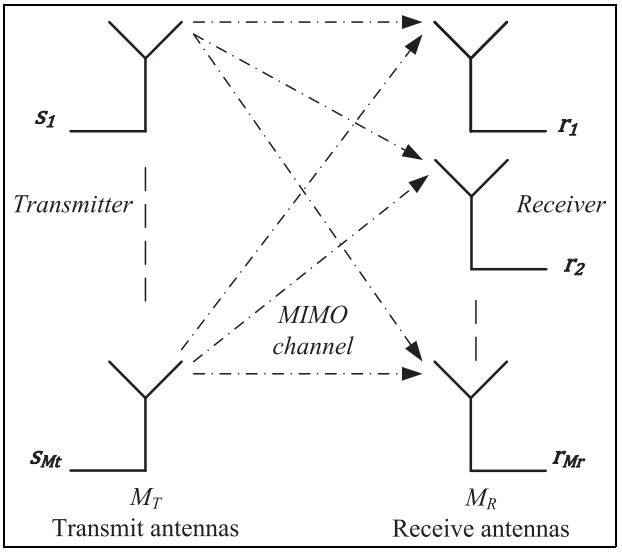


**Figure 7.** The MIMO-OCDM system.

The CSI from the receiver is fed back to the transmitter to optimize these rotations with the assumption that they are on time and errorless for easiness. EO-STBC can be simply derived in MCM schemes such as OFDM or OCDM[15] in broadband scenarios.

Multicarrier EO-STBC configuration block diagram is shown in Figure 6 where the data vector $\boldsymbol{d}_n$ dimension is equal to the number of dynamic subcarriers $N_a$. MCM transmission symbols $\boldsymbol{s}_{i,n}$, $i = 0, \ldots, 3$ produced from the four antennas are defined over two successive symbol periods as

$$\boldsymbol{s}_{j,n} = \begin{cases} \boldsymbol{d}_n, & n \text{ is even} \\ \boldsymbol{d}_n^*, & n \text{ is odd} \end{cases} \tag{39}$$

$$\boldsymbol{s}_{(j+2),n} = \begin{cases} \boldsymbol{d}_{n+1}, & n \text{ is even} \\ \boldsymbol{d}_{n+1}^*, & n \text{ is odd} \end{cases} \tag{40}$$

where $j \in \{0, 1\}$. The first and third antenna signal includes an adjustment due to phase rotations as shown in Figure 6, where the phase rotations are given by

$$\boldsymbol{\phi}_n = \text{diag}\left\{e^{j\varphi_{1,n}}, \ldots, e^{j\varphi_{N_a,n}}\right\} \tag{41}$$

$$\boldsymbol{\theta}_n = \text{diag}\left\{e^{j\vartheta_{1,n}}, \ldots, e^{j\vartheta_{N_a,n}}\right\} \tag{42}$$

which apply rotation to subcarriers. Using the corresponding multicarrier channel model $\boldsymbol{U}_{i,n} = \boldsymbol{P}^H\boldsymbol{F}_\alpha \boldsymbol{H}_{i,n}\boldsymbol{F}_{-\alpha}\boldsymbol{P}$ to describe the four transmitting channel paths linking the transmitter and the receiver, as maintained in Figure 6, the vector $\tilde{r}_n$ is the received signal which is given by

$$\tilde{\boldsymbol{r}}_n = \boldsymbol{U}_{0,n}\boldsymbol{\phi}_n\boldsymbol{s}_{0n} + \boldsymbol{U}_{1,n}\boldsymbol{s}_{1,n} + \boldsymbol{U}_{2,n}\boldsymbol{\theta}_n\boldsymbol{s}_{2,n} + \boldsymbol{U}_{3,n}\boldsymbol{s}_{3,n} + \tilde{\boldsymbol{z}}_n \tag{43}$$

where $\tilde{\boldsymbol{z}}_n = \boldsymbol{P}^H\boldsymbol{F}_\alpha\boldsymbol{z}$ and $\tilde{z}_n$ is a zero-mean white complex Gaussian circularly symmetric random noise vector with covariance $E\{\tilde{\boldsymbol{z}}_n\tilde{\boldsymbol{z}}_n^H\} = \sigma^2\boldsymbol{I}_{N_a}$.

Collecting data over two consecutive OCDM symbol periods, the received vector signal can be written as

$$\begin{bmatrix} \tilde{\boldsymbol{r}}_n \\ \tilde{\boldsymbol{r}}_{n+1}^* \end{bmatrix} = \boldsymbol{G}_n \begin{bmatrix} \boldsymbol{d}_n \\ \boldsymbol{d}_{n+1} \end{bmatrix} + \begin{bmatrix} \tilde{\boldsymbol{z}}_n \\ \tilde{\boldsymbol{z}}_{n+1}^* \end{bmatrix} \tag{44}$$

where $\boldsymbol{G}_n$ is given by

$$\boldsymbol{G}_n = \begin{bmatrix} \boldsymbol{U}_{0,n}\boldsymbol{\phi}_n + \boldsymbol{U}_{1,n} & \boldsymbol{U}_{2,n}\boldsymbol{\theta}_n + \boldsymbol{U}_{3,n} \\ \boldsymbol{U}^*_{2,n+1}\boldsymbol{\theta}_{n+1} + \boldsymbol{U}^*_{3,n+1} & -\boldsymbol{U}^*_{0,n+1}\boldsymbol{\emptyset}_{n+1} - \boldsymbol{U}^*_{1,n+1} \end{bmatrix} \tag{45}$$

It is worth noticing that, if the MISO channel is static and the DFrFT-OCDM configuration is used with chirp rate $\alpha = \pm 1$, the corresponding system channel matrices $\boldsymbol{U}_{i,n}$ become diagonal, guaranteeing that

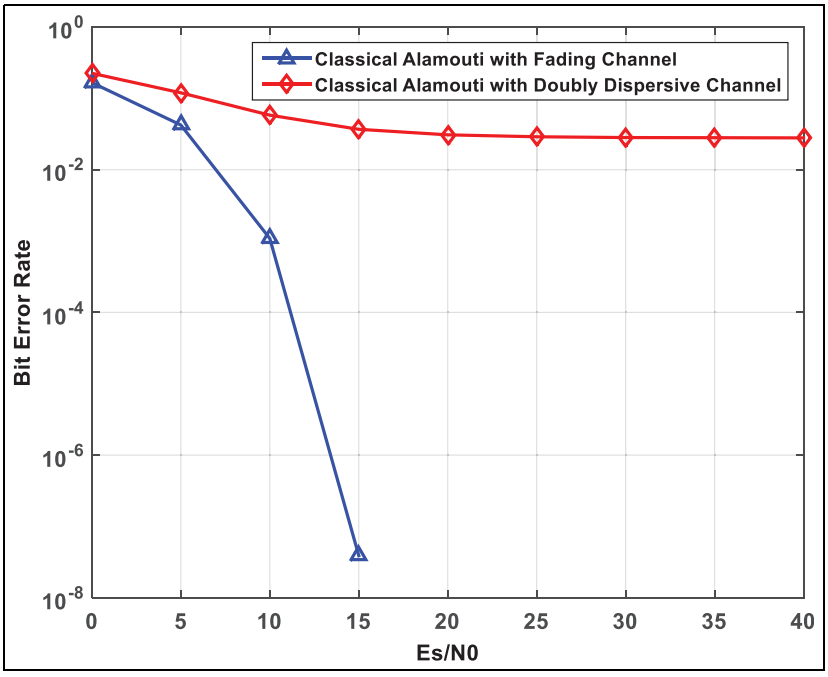


**Figure 8.** Uncoded BER comparison for the classical Alamouti space–time coded OFDM system with time-invariant and time-variant channels.

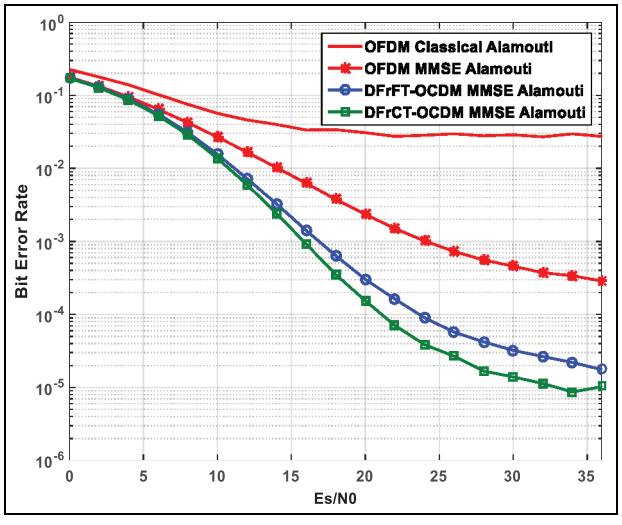


**Figure 9.** Uncoded BER comparison for the classical Alamouti space–time coded OFDM system with different Alamouti STBC systems based on OFDM, DFrFT, and DFrCT-OCDM using MMSE equalizer under time-variant channel.

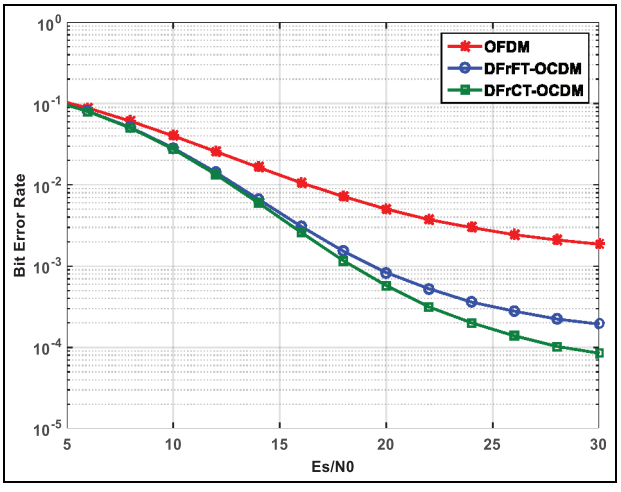


**Figure 10.** Uncoded BER comparison for different Alamouti space–time coded systems based on OFDM, DFrFT, and DFrCT-OCDM using low-complexity MMSE equalizer.

subcarriers can be EO-STBC decoded separately and ICI is ignored.

## Proposed space–time decoding

In a frequency- and time-selective fading channel scenario, Doppler shift destroys the orthogonality between subcarriers and the OFDM system is unable to diagonalize the system matrix in equation (45). Consequently, the coupling between at least the adjacent subcarriers is proposed, leading to degradation in the system performance.

Symbols can be detected by ignoring ICI under the near-stationary channel scenario with low Doppler shift character, using only the elements on the main diagonal of the channel transfer matrix. Thus, the OFDM

system can be employed due to its low complexity. This indicates that any off-diagonal contents in the corresponding channel matrices $\boldsymbol{U}_{i,n}$ will be disregarded. The diversity gain can be improved greatly, by guaranteeing that the angles in $\boldsymbol{\phi}_n$ and $\boldsymbol{\theta}_n$ increase the on-diagonal terms of the reduced system matrix to the maximum.

Low Doppler shift EO-STBC receivers can combat cross-talk on each subcarrier separately to enhance the feedback diversity gain. In STBC systems, the channels are generally expected to remain in block static form. In this case, frequency-domain channel submatrices are orthogonal which imply that the symbols can be decoded simply by the simple maximum-likelihood (SML) algorithm; the complexity of the SML algorithm is directly proportional to the number of subcarriers. However, in time-selective fading channels, frequency-domain channel submatrices become no longer orthogonal, so decoding to decrease the effect of cross-talk can be performed by the JML algorithm, which has more complexity than some algorithms such as ZF and DF.[1,2]

On the other hand, for higher Doppler shift in order to soften the effect of high Doppler shift on the EO-STBC decoding performance, equalization is needed and the angle feedback to the transmitter is not required. In the next section, a novel EO-STBC scheme will be presented.

### Open-loop EO-STBC decoding with equalization

The EO-STBC system combined with the OCDM performance under higher Doppler shift conditions can be improved using equalization which raises the receiver's complication; however, it eliminates the need for the angle feedback to the transmitter. Consequently, the beam steering matrices are simply set to be identity matrices $\boldsymbol{I}$ as $\boldsymbol{\phi}_n = \boldsymbol{\theta}_n = \boldsymbol{I}$.

*OCDM EO-STBC system low-complexity equalizers.* Low-complexity equalizers can be used with the OCDM EO-STBC system such as banded linear block MMSE, $LDL^{\mathrm{H}}$, and LSMR equalizers which were described in previous studies.[3,16,23,34,35]

Assuming the perfect channel knowledge, a block MMSE equalizer is defined based on the system matrix $\boldsymbol{G}_n$ in equation (45) that is a $2\times 2$ block matrix of $N\times N$ nearly banded matrices. $\boldsymbol{G}_n$ can be transferred to a $2\times 2$ block matrix of $N\times N$ banded matrices, using the masked matrix $\boldsymbol{M}$ which is defined in equation (18) to reduce the equalization process complexity

$$\boldsymbol{B}_n = \begin{bmatrix} \boldsymbol{M} & \boldsymbol{M} \\ \boldsymbol{M} & \boldsymbol{M} \end{bmatrix} \odot \boldsymbol{G}_n \tag{46}$$

where $\boldsymbol{B}_n$ is the banded system matrix version of $\boldsymbol{G}_n$. The received data can be rewritten as

$$\begin{bmatrix} \tilde{\boldsymbol{r}}_n \\ \tilde{\boldsymbol{r}}^*_{n+1} \end{bmatrix} = \boldsymbol{B}_n \begin{bmatrix} \boldsymbol{d}_n \\ \boldsymbol{d}_{n+1} \end{bmatrix} + \begin{bmatrix} \tilde{\boldsymbol{z}}_n \\ \tilde{\boldsymbol{z}}^*_{n+1} \end{bmatrix} \tag{47}$$

where $\boldsymbol{B}_n$ can be re-arranged using the permutation matrix $\mathcal{P}(2N\times 2N)$, where the data from different transmitting antennas and the same subcarriers are assembled together, and the received data from the same subcarriers in two successive OCDM symbol periods are discretely assembled together

$$\mathcal{P}\begin{bmatrix} \tilde{\boldsymbol{r}}_n \\ \tilde{\boldsymbol{r}}^*_{n+1} \end{bmatrix} = \mathcal{P}\boldsymbol{B}_n\mathcal{P}^T\mathcal{P}\begin{bmatrix} \boldsymbol{d}_n \\ \boldsymbol{d}_{n+1} \end{bmatrix} + \mathcal{P}\begin{bmatrix} \tilde{\boldsymbol{z}}_n \\ \tilde{\boldsymbol{z}}^*_{n+1} \end{bmatrix} \tag{48}$$

Similar to equation (21), we can define the MMSE equalizer as

$$\boldsymbol{W}_{n,MMSE} = \boldsymbol{B}_n^H\left(\boldsymbol{B}_n\boldsymbol{B}_n^H + \gamma^{-1}\boldsymbol{I}_{N_a}\right)^{-1} \tag{49}$$

where $\gamma$ is the signal-to-noise ratio (SNR) at the input of the equalizer, supposing that the noise is white Gaussian noise. The matrix inversion in equation (49) needs $\mathcal{O}(8N_a^3)$ complex operations, which is not applied for large values of $2N_a$. The ZF equalizer $\boldsymbol{W}_{n,ZF}$ can be calculated from equation (49) for the special case

$$\boldsymbol{W}_{n,ZF} = \boldsymbol{W}_{n,MMSE}|_{\gamma\to\infty} = \boldsymbol{B}_n^H\left(\boldsymbol{B}_n\boldsymbol{B}_n^H\right)^{-1} \tag{50}$$

Similar to equation (49), the matrix inversion in equation (50) is in the order of $\mathcal{O}(8N_a^3)$ and it enhances the noise effect that degrades the system performance. It is obvious that using the low-complexity equalizers decreases the system complexity at almost the same level of system's performance.

*Low-complexity equalizers' realization.* The matrix inversion for equalization (equation (49)) needs a considerable number of $\mathcal{O}(8N_a^3)$ complex processes, which is regarded as excessive for great $2N_a$. Applying $LDL^{\mathrm{H24}}$ matrix factorization in computing either ZF or MMSE solutions in equations (49) and (50) will reduce the number of complex processes related to standard matrix inversion methods, such as Gaussian elimination to $\mathcal{O}(8Q^2 + 22Q + 4)2N_a$ complex processes.

The LSMR realization of either ZF or MMSE solution needs $\mathcal{O}(2N_a(Q+1))$ complex processes for each iteration, leading to a total of $\mathcal{O}(2N_a(Q+1)i)$ complex processes. LSMR can reach the same precision of matrix inversion with a significantly lower number of complex processes, hence leading to a general decrease in complexity.

## A novel MIMO-OCDM system

In the last two sections, STBC MISO systems were investigated in detail under the doubly dispersive fading channel, and the combined system with the novel

OCDM MCM was introduced. In this section, combining the MIMO system with the OCDM system is investigated under the doubly dispersive channel scenario conditions.

## MIMO-OCDM system model

Consider a MIMO-OCDM system with $M_T$ transmitting antennas, $M_R$ receiving antennas, and $N$ subcarriers as shown in Figure 7. The $M_T M_R$ SISO channels between the transmitting and receiving antennas are considered to be uncorrelated time- and frequency-selective fading and characterized by the same fading statistics, with the CP length $L$ being larger than the maximum delay spread; the received vector at the $j$th receiving antenna, after inverse transformation (IDFrFT–IDFrCT) and CP removal can be expressed as

$$\boldsymbol{r}_j = \sum_{i=1}^{M_T} \tilde{\boldsymbol{H}}_{i,j}\boldsymbol{d}_i + \tilde{\boldsymbol{z}}_j \tag{51}$$

where $\boldsymbol{r}_j$ is the received vector with $N \times 1$ dimensions, $\tilde{\boldsymbol{H}}_{i,j}$ is the fractional domain channel matrix with $N \times N$ dimensions between the $j$th and the $i$th receiving and transmitting antennas, respectively, $\boldsymbol{d}_i$ is the OCDM fractional domain data block with $N \times 1$ dimensions, transmitted by the $i$th transmitting antenna, where the data transmitted from different antennas are independent, and $\tilde{\boldsymbol{z}}_j$ is the noise vector of the $j$th receiving antenna in the fractional domain with $N \times 1$ dimensions, given by $\tilde{\boldsymbol{z}}_j = \boldsymbol{F}_\alpha \boldsymbol{z}_j$. Each fractional domain channel matrix can be stated as

$$\tilde{\boldsymbol{H}}_{i,j} = \boldsymbol{F}_\alpha \boldsymbol{H}_{i,j} \boldsymbol{F}_\alpha^H \tag{52}$$

where $\boldsymbol{H}_{i,j}$ is the $N \times N$ time-domain channel matrix between the $j$th and $i$th receiving and transmitting antennas, respectively, and $\boldsymbol{F}_\alpha$ is the $N \times N$ unitary DFrFT or DFrCT matrix, with the fractional order $\alpha$. In time-varying channels, both DFrFT and DFrCT cannot diagonalize $\boldsymbol{H}_{i,j}$. As a consequence, a firm measure of ICI is existent which degrades the system performance.

The transmitted data vector $\boldsymbol{d}_n = [d_0\ d_1\ \ldots\ d_{N_a-1}]^T$ is permuted by the binary matrix $\boldsymbol{P} \in \mathbb{Z}^{N \times N_a}$ $\boldsymbol{P} \in \mathbb{Z}^{N \times N_a}$ which allocates a data vector $\boldsymbol{d}_n \in \mathbb{C}^{N_a}$ to $N$ subcarriers, where only $N_a$ are active due to

$$\boldsymbol{P} = \begin{bmatrix} 0_{N_a \times (N-N_a)/2} & \boldsymbol{I}_{N_a} & 0_{N_a \times (N-N_a)/2} \end{bmatrix} \tag{53}$$

where $\boldsymbol{P}$ is the $N \times N$ matrix that introduces the $N - N_a$ frequency guard bands. All the received vectors by the $M_R$ antennas $\{\boldsymbol{r}_j\}_{i=1}^{M_R}$ can be collected in a single vector

$$\underline{\boldsymbol{r}} = \underline{\tilde{\boldsymbol{H}}}\underline{\boldsymbol{d}} + \underline{\boldsymbol{z}} \tag{54}$$

where $\underline{\boldsymbol{r}} = [\boldsymbol{r}_1^T \quad \ldots \quad \boldsymbol{r}_{M_R}^T]^T$, $\underline{\boldsymbol{d}} = [\boldsymbol{d}_1^T \quad \ldots \quad \boldsymbol{d}_{M_T}^T]^T$, $\underline{\tilde{\boldsymbol{H}}}$ is specified by

$$\underline{\tilde{\boldsymbol{H}}} = \begin{bmatrix} \tilde{\boldsymbol{H}}_{1,1} & \cdots & \tilde{\boldsymbol{H}}_{1,M_T} \\ \vdots & \ddots & \vdots \\ \tilde{\boldsymbol{H}}_{M_R,1} & \cdots & \tilde{\boldsymbol{H}}_{M_R,M_T} \end{bmatrix} \tag{55}$$

and $\underline{\boldsymbol{z}} = [\boldsymbol{z}_1^T \quad \ldots \quad \boldsymbol{z}_{M_R}^T]^T$ with covariance expressed as $\boldsymbol{Co}_{zz} = \boldsymbol{I}_{M_R} \otimes \sigma_\vartheta^2$.

There is a need for a permutation matrix to deal with the MIMO system $\boldsymbol{\mathcal{P}}_{(M,N)}$ as the $MN \times MN$ matrix that contains 1's in the positions given by

$$\{(i+1, i/M + 1 + Ni_{\mathrm{mod}M})\}_{i=0}^{MN-1} \tag{56}$$

and 0's elsewhere. Using the permutation matrix $\boldsymbol{\mathcal{P}}_{(M,N)}$ to permute the received vector in equation (54), we obtain

$$\begin{aligned} \boldsymbol{\mathcal{R}} = \boldsymbol{\mathcal{P}}_{(M_R,N)}\underline{\boldsymbol{r}} = \left(\boldsymbol{\mathcal{P}}_{(M_R,N)}\underline{\tilde{\boldsymbol{H}}}\boldsymbol{\mathcal{P}}_{(M_T,N)}^T\right)\left(\boldsymbol{\mathcal{P}}_{(M_T,N)}\underline{\boldsymbol{d}}\right) \\ + \left(\boldsymbol{\mathcal{P}}_{(M_R,N)}\underline{\boldsymbol{z}}\right) \end{aligned} \tag{57}$$

$$\boldsymbol{\mathcal{R}} = \boldsymbol{\mathcal{H}}\underline{\boldsymbol{d}} + \underline{\boldsymbol{z}} \tag{58}$$

where $\boldsymbol{\mathcal{R}}$ is the permuted received vector, $\boldsymbol{\mathcal{H}}$ is the permuted fractional MIMO channel matrix, $\underline{\boldsymbol{d}}$ is the permuted data vector, and $\underline{\boldsymbol{z}}$ is the permuted noise vector.

Both equations (54) and (57) prove that the received data from two different transmitters at the same subcarrier are adjacent and close enough, to assume that they both hold the same transmitted data property. As a result, it is acceptable to claim that the tops and the bottoms of the bandwidths for both of them are close to each other at the top and at the bottom of $\underline{\boldsymbol{d}}$. It is clear that the estimation of the data vector $\underline{\boldsymbol{d}}$ will require complicated equalizers.

## MIMO-OCDM system equalization

The linear ZF and MMSE estimates[5,36] can be derived by minimizing $E\{\| \boldsymbol{d}_n - \boldsymbol{W}\boldsymbol{\mathcal{R}} \|\}$, thus yielding

$$\hat{\boldsymbol{d}}_{ZF} = \boldsymbol{\mathcal{H}}^+ \boldsymbol{\mathcal{R}} \tag{59}$$

$$\hat{\boldsymbol{d}}_{MMSE} = \boldsymbol{\mathcal{H}}^H \left(\boldsymbol{\mathcal{H}}\boldsymbol{\mathcal{H}}^H + \mathcal{C}\boldsymbol{o}_{zz}\right)^{-1} \boldsymbol{\mathcal{R}} \tag{60}$$

where $\mathcal{C}\boldsymbol{o}_{zz}$ is the permuted noise covariance vector $\mathcal{C}\boldsymbol{o}_{zz} = \boldsymbol{P}_{(M_R,N_a)}\boldsymbol{Co}_{zz}\boldsymbol{P}_{(M_R,N_a)}$; $\hat{\boldsymbol{d}}_{ZF}$ and $\hat{\boldsymbol{d}}_{MMSE}$ are the estimated data after ZF and MMSE equalization, respectively; $\boldsymbol{\mathcal{H}}^H$ is the fractional MIMO channel matrix conjugate transpose in the fractional domain; and $\boldsymbol{\mathcal{H}}^+$ is the Moore–Penrose pseudo-inverse of the fractional MIMO channel matrix.

$\hat{\boldsymbol{d}}_{MMSE}$ is the permuted version of the estimated data $\hat{\boldsymbol{d}}$ which can be recovered by

$$\hat{\boldsymbol{d}} = \boldsymbol{\mathcal{P}}^T \hat{\boldsymbol{d}}_{MMSE} \tag{61}$$

ZF equalizer performance is reduced because of the noise enhancement. On the other hand, the MMSE equalizer gives the best performance among all types of linear equalizers;[37] however, it is very complicated due to MIMO channel matrix inversion.

The permuted MIMO channel matrix $\boldsymbol{\mathcal{H}}$ is nearly banded which implies that the greatest amount of the ICI arises from the adjacent subcarriers. Consequently, the nearly banded structure of $\tilde{\boldsymbol{H}}_{i,j}$ indicates that $\boldsymbol{\mathcal{H}}$ is nearly block-banded, resulting in the validity of using low-complexity equalizers with the MIMO-OCDM system.

### *MIMO-OCDM system with low-complexity equalization*

The MIMO-OCDM channel matrix $\boldsymbol{\mathcal{H}}$ can be approximated by its banded version, expressed as

$$\boldsymbol{\mathcal{B}}_{(Q)} = \boldsymbol{\mathcal{M}} \odot \boldsymbol{\mathcal{H}} \tag{62}$$

where $\odot$ represents the element-wise multiplication, $\boldsymbol{\mathcal{M}} = \boldsymbol{M} \otimes \boldsymbol{I}_{M_R \times M_T}$ with $\boldsymbol{M}$ being a binary masking matrix that was given in equation (18), and the $Q$ parameter defines the size of the block band, which can be selected as in SISO-OFDM. It will be shown that the $Q$ parameter is used in the equalizers to compromise between complexity and performance.

$\boldsymbol{\mathcal{B}}_{(Q)}$ is the banded fractional MIMO channel matrix $\boldsymbol{\mathcal{H}}$ which permits the use of low-complexity equalizers called banded equalizers. Depending on the masked channel matrix, the definition of the MMSE equalizer can be given by

$$\mathcal{W}_{n,MMSE} = \boldsymbol{\mathcal{B}}_n^H \left(\boldsymbol{\mathcal{B}}_n \boldsymbol{\mathcal{B}}_n^H + \mathcal{C}o_{zz}\right)^{-1} \tag{63}$$

The estimated data vector will be given by

$$\hat{\boldsymbol{d}}_{MMSE} = \mathcal{W}_{n,MMSE} \boldsymbol{\mathcal{R}} = \boldsymbol{\mathcal{B}}_n^H \left(\boldsymbol{\mathcal{B}}_n \boldsymbol{\mathcal{B}}_n^H + \mathcal{C}\boldsymbol{o}_{zz}\right)^{-1} \boldsymbol{\mathcal{R}} \tag{64}$$

The $LDL^H$ factorization algorithm and all the LSMR algorithm equalizer versions can be used. Simulation for different equalizers will be shown in the next section.

## Selection of optimal order $\alpha$

We will now investigate the effect of the fractional order $\alpha$ on the DFrCT-OCDM multicarrier system performance. To improve the multicarrier system performance, $\alpha$ should be chosen such that the subchannel carrier frequency variation should match the fast time–frequency distortion of the channel. Selecting $\alpha$ depends on the number of subcarriers $N$, time sample interval $T_s$, the Doppler shift $f_D$, the number of resolvable channel paths, and the channel power delay profile. Offline optimization of $\alpha$ for DFrFT-OCDM was proposed in Martone[6] using calculations of the channel statistical expectations. The same method can be used with the DFrCT-OCDM by extracting the channel properties at the receiver; define the optimum $\alpha$ which gives the lowest ICI and then feedback the $\alpha$ value to the transmitter.

## Simulation and results

The uncoded BER performances of the systems are investigated by means of simulation. The channels used in simulation are Rayleigh fading independent channels with exponential power delay profile and Jakes' Doppler spectrum. The root-mean-square (RMS) delay spread of the channel, normalized to the sampling period $T_S$, is $\sigma = 3$ with maximum Doppler frequency $f_D = 0.15\Delta f$. The carrier frequency is $f_C = 10\,\text{GHz}$ and the subcarrier spacing is $\Delta f = 20\,\text{kHz}$. This Doppler frequency corresponds to a high mobile speed $V = 324\,\text{km/h}$. This channel model uses the same statistics as in previous studies.[3,4,22]

### *Alamouti MISO OCDM system performance*

The decoding algorithms proposed previously are now inspected and compared by means of simulation. The Alamouti space–time coded system based on OFDM, DFrFT-OCDM, and DFrCT-OFDM with the same specifications as in the SISO scheme was considered.

To evaluate the performance of the suggested system, an OFDM transmission is used with quadrature phase shift keying (QPSK) modulation, $N = 128$ subcarriers of which $N_a = 96$ are active and a CP of length $L = 8$. Simulations are performed over an ensemble of $10^5$ Rayleigh fading channels defined by an exponential power delay profile with an RMS delay spread of three sampling periods. Figure 8 shows the comparison of the BER performance of the classical Alamouti space–time coded OFDM system with those of time-invariant and time-variant channels. It is obvious that the classical Alamouti decoding fails totally because of the doubly dispersive channel that destroys the orthogonality among the subcarriers.

Figure 9 shows the comparison of the BER performance of the different Alamouti space–time coded systems based on OFDM, DFrFT, and DFrCT using MMSE equalizer in decoding with the classical Alamouti decoding system, based on OFDM under time-variant channel. Using equalization for the Alamouti system decoding improves the system performance compared to the OFDM case under high-mobility conditions (doubly selective channel); in fact, the proposed system using DFrCT-OCDM provides

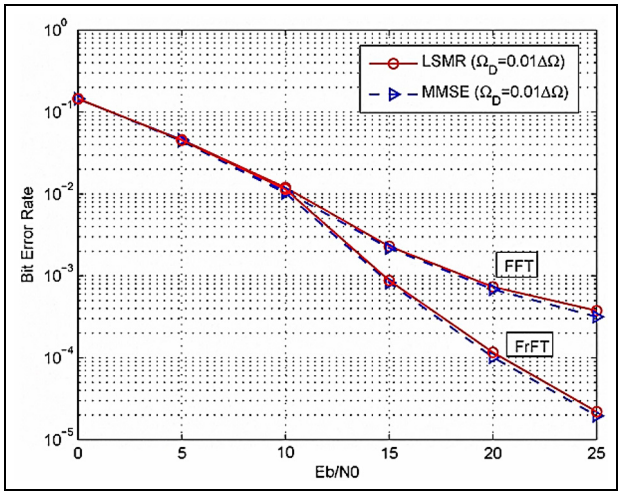


**Figure 11.** Multicarrier EO-STBC system based on OCDM and classical OFDM with block equalization BER comparison.

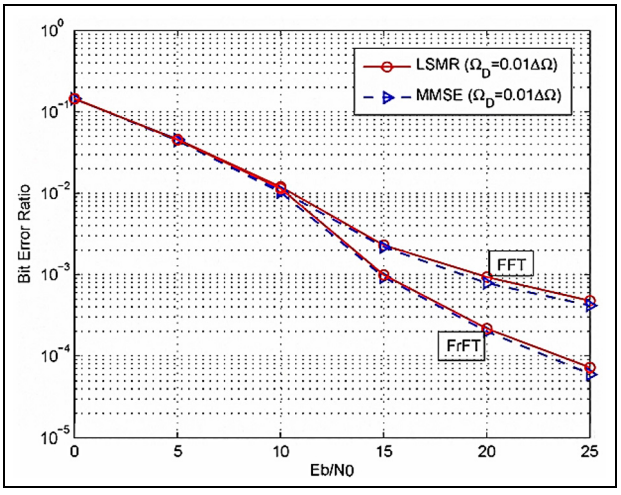


**Figure 12.** Multicarrier EO-STBC system based on OCDM and classical OFDM with banded equalization ($Q = 12$) BER comparison.

better performance even from the DFrFT-OCDM system.

Comparison between the proposed DFrFT-OCDM, DFrCT-OCDM, and OFDM systems using low-complexity equalizers for Alamouti coding is shown in Figure 10.

It is clear that using a low-complexity equalizer degrades the system performance, because the banded equalizers have an error level because of the band rough calculation error of the channel, which can be improved dramatically by increasing the $Q$ parameter in equation (62) with the cost of increasing the system complexity.

## *EO-STBC OCDM MISO transceiver performance*

The proposed multicarrier EO-STBC DFrCT-OCDM MISO transceiver is investigated using simulation under doubly dispersive fading conditions, and then a performance comparison between the novel system and the EO-STBC OFDM MISO transceiver is made.

In Figure 11, a performance comparison between the OCDM and OFDM EO-STBC systems using a block equalizer is shown, and Figure 12 illustrates the results of using a less complex method that applies an equalizer limited to working on $Q = 12$ of the permutation system matrix $G_n$.

As shown in Figures 11 and 12, the BER performance for the OFDM and DFrFT-OCDM systems is almost the same up to approximately 10 dB $E_B/N_0$ due to additive white Gaussian noise (AWGN). At higher $E_B/N_0$, the BER performance degrades in the banded equalizer case because of the error in neglecting off-diagonals larger than $Q = 12$. In the OCDM case, most of the energy within the matrix is intense nearby the main diagonal[3] as it can reach an improved performance than the OFDM-based system even with almost the same complexity. The approach labeled MMSE in Figure 11 represents a typical inversion of the approximate channel matrix $B_n$, while the LSMR scheme implements an MMSE strategy, with condensed complexity due to the LSMR iterative nature.

## *MIMO-OCDM system performance*

The proposed MIMO-OCDM transceiver will be investigated using simulation under doubly dispersive fading conditions, and a performance comparison between the novel system and the MIMO-OFDM transceiver is made. The simulation is carried out over 100,000 different symbols and different channels. A comparison between the MIMO-OCDM and the MIMO-OFDM systems is carried by using two transmitting antennas and three receiving antennas, with the block MMSE equalizer as shown in Figure 13. From the figure, it is clear that the MIMO-OCDM systems are much improved than the MIMO-OFDM system and the MIMO-DFrCT system is improved than the MIMO-DFrFT system. It can be observed from Figure 13 that the OCDM MIMO systems outperform the OFDM system in the 1% uncoded BER area by 3 dB and in the 0.1% uncoded BER area by 2.5 dB. It is clear that the DFrCT-OCDM system outperforms the DFrCT-OCDM system in the 0.1% uncoded BER area by 0.5 dB.

Comparison between the MIMO-DFrCT and the SISO-DFrCT system is made using the block MMSE equalizer as shown in Figure 14. It is obvious that the MIMO-DFrCT system is better than the SISO-DFrCT system because of the diversity gained for the MIMO system.

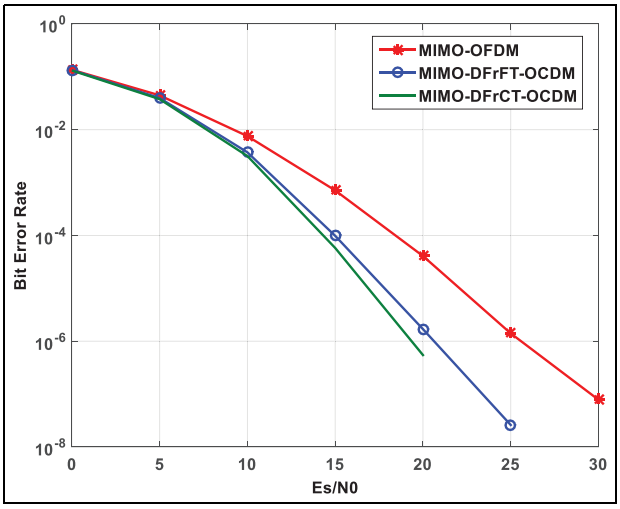


**Figure 13.** The MIMO system performance with two transmitting antennas and three receiving antennas using MMSE equalizer.

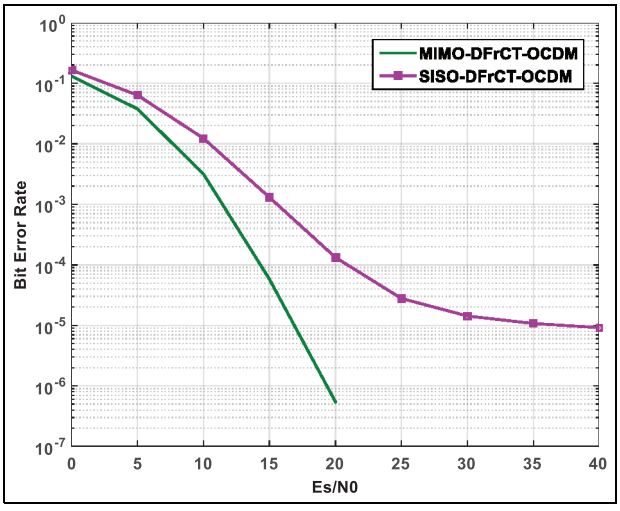


**Figure 14.** BER comparison between the MIMO and SISO DFrCT-OCDM systems with two transmitting antennas and three receiving antennas using MMSE equalizer.

Comparison between the MIMO-OCDM and MIMO-OFDM systems is made using two transmitting antennas and three receiving antennas with the low-complexity banded MMSE equalizer, as shown in Figure 15. From the figure, it is clear that the MIMO-OCDM systems are much better than the MIMO-OFDM systems and the MIMO-DFrCT system is better than the MIMO-DFrFT system. It is also clear that the performance of the banded low-complexity MMSE equalizer is less than that of the MMSE equalizer due to banded approximation.

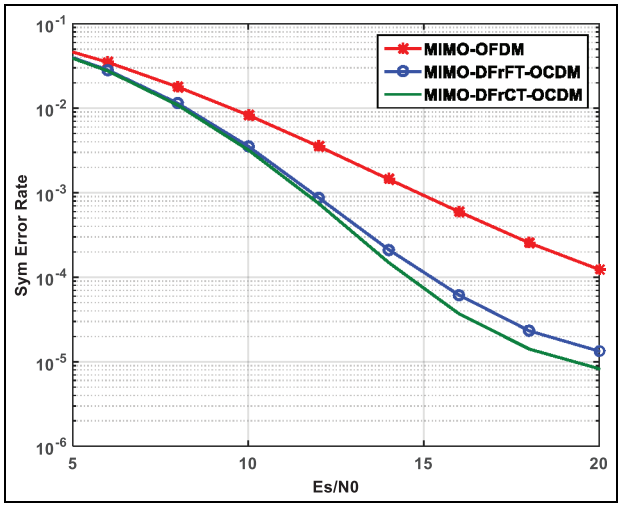


**Figure 15.** The MIMO system performance with two transmitting antennas and three receiving antennas using banded low-complexity MMSE equalizer.

## Conclusion

In this article, three novel systems have been introduced which are Alamouti STBC MISO MIMO-MCM system, EO-STBC MISO MCM system, and MIMO system, based on the OCDM MCM systems. MISO systems based on Alamouti decoding were investigated and a combination with OCDM was proposed; as a result, the proposed combined system, that is, MISO OCDM, improved the system performance. To provide a better understanding of the proposed system, EO-STBC transmission was studied over a frequency- and time-dispersive channel and then compared with the other systems. In addition, a multicarrier scheme was deployed to soften the time-based dispersion resulted from frequency spreading due to Doppler shift, which could lead to a major performance degradation because of losing the subcarrier decoupling. Usually, in the case of low Doppler shift and near-static channel situations, ICI can be ignored, while in the case of higher Doppler shift a general multicarrier system based on the OCDM with equalization can be used. The results show that OCDM can hold more channel energy along the main diagonal, compared to classical OFDM, which leads to improved system performance and decreased equalization complexity. Finally, the MIMO-OCDM systems were proposed to improve the performance of the MIMO-MCM systems under doubly dispersive channels. The novel MIMO and MISO-OCDM systems were investigated using low-complexity equalizers and shown to provide better performance than the MIMO and MISO OFDM systems.

Future work is directed to combine the network coding technique on the system to exploit the significant

advantages of this technique, in terms of channel capacity and BER, and to reduce the automatic repeat request (ARQ) as proved in Attar and colleagues.[38–41]

## Author contributions

A.A.A.S., H.H.A., and M.R.K. prepared the comparative analysis report. H.H.A. and B.K. used the selected tools for performing simulations. A.A.A.S. and H.H.A. wrote the manuscript and M.R.K. and B.K. suggested various changes.

## Declaration of conflicting interests

The author(s) declared no potential conflicts of interest with respect to the research, authorship, and/or publication of this article.

## Funding

The author(s) received no financial support for the research, authorship, and/or publication of this article.

## ORCID iD

Hani Attar https://orcid.org/0000-0001-8028-7918

## References

1. Nassiri M and Baghersalimi G. Comparative performance assessment between FFT-based and FRFT-based MIMO-OFDM systems in underwater acoustic communications. *IET Commun* 2018; 12: 719–726.
2. Chen Y, Clemente C, Soraghan J, et al. Fractional Fourier based sparse channel estimation for multicarrier underwater acoustic communication system. In: *2016 sensor signal processing for defence (SSPD)*, Edinburgh, 22–23 September 2016, pp.1–5. IEEE.
3. Solyman AAA, Weiss S, Soraghan JJ, et al. Low-complexity LSMR equalisation of FrFT-based multicarrier systems in doubly dispersive channels. In: *2011 IEEE international symposium on signal processing and information technology (ISSPIT)*, Bilbao, 14–17 December 2011, pp.461–465. New York: IEEE.
4. Luca Rugini PB and Leus G. Low-complexity banded equalizers for OFDM systems in Doppler spread channels. *EURASIP J Appl Signal Process* 2006; 2006: 67404.
5. Rugini L, Banelli P, Leus G, et al. Simple equalization of time-varying channels for OFDM. *IEEE Commun Lett* 2005; 9: 619–621.
6. Martone M. A multicarrier system based on the fractional Fourier transform for time-frequency-selective channels. *IEEE T Commun* 2001; 49: 1011–1020.
7. Kaye A and George D. Transmission of multiplexed PAM signals over multiple channel and diversity systems. *IEEE Trans Comm Techn* 1970; 18(5): 520–526.
8. Brandenburg LH and Wyner AD. Capacity of the Gaussian channel with memory: the multivariate case. *Bell Syst Tech J* 1974; 53: 745–778.
9. Alamouti SM. A simple transmit diversity technique for wireless communications. *IEEE J Selected Areas Commun* 1998; 16: 1451–1458.
10. Akhtar J and Gesbert D. Partial feedback based orthogonal block coding. In: *The 57th IEEE semiannual vehicular technology conference (VTC 2003—Spring)*, Jeju, South Korea, 22–25 April 2003, vol. 1, pp.287–291. New York: IEEE.
11. Akhtar J and Gesbert D. Extending orthogonal block codes with partial feedback. *IEEE T Wirel Commun* 2004; 3: 1959–1962.
12. Agrawal D, Tarokh V, Naguib A, et al. Space-time coded OFDM for high data-rate wireless communication over wideband channels. In: *48th IEEE vehicular technology conference (VTC '98), 1998*, Ottawa, ON, Canada, 21 May 1998, vol. 3, pp.2232–2236. New York: IEEE.
13. Farrukh FuD, Baig S and Mughal MJ. MMSE equalization for discrete wavelet packet based OFDM. In: *Third international conference on electrical engineering 2009 (ICEE '09)*, Lahore, Pakistan, 9–11 April 2009, pp.1–4. New York: IEEE.
14. Attar H and Solyman A. A proposed orthogonal chirp division multiplexing (OCDM) multicarrier transceiver based on the discrete fractional cosine transform. *J Comp Commun* 2017; 5(2): 34–47.
15. Hussin MN, Solyman AAA, Weiss S, et al. FrFT-based EO-STBC multicarrier system for transmission over doubly-dispersive channels. In: *2012 international symposium on wireless communication systems (ISWCS)*, Paris, 28–31 August 2012, pp.686–690. New York: IEEE.
16. Solyman AAA, Weiss S and Soraghan JJ. A novel orthogonal chirp division multiplexing (OCDM) multicarrier transceiver based on the discrete fractional cosine transform. In: *2013 Mosharaka international conferences on 3rd international conference on wireless communications and mobile computing (MIC-WCMC)*, Valencia, Spain, 14–16 June 2013.
17. Candan C, Kutay MA, Ozaktas HM, et al. The discrete fractional Fourier transform. *IEEE T Signal Proces* 2000; 48: 1329–1337.
18. Wang J and Wang J. Feature extraction method of fractional cosine and sine transform for speaker recognition. In: *12th IEEE international conference on electronics, circuits and systems (ICECS 2005)*, Gammarth, Tunisia, 11–14 December 2005, pp.1–4. New York: IEEE.
19. Soo-Chang P and Min-Hung Y. The discrete fractional cosine and sine transforms. *IEEE T Signal Proces* 2001; 49: 1198–1207.
20. Soo-Chang P and Jian-Jiun D. Fractional cosine, sine, and Hartley transforms. *IEEE T Signal Process* 2002; 50: 1661–1680.
21. Paige CC and Saunders MA. LSQR: an algorithm for sparse linear equations and sparse least squares. *ACM T Math Software* 1982; 8: 43–71.
22. Rugini L and Banelli P. Banded equalizers for MIMO-OFDM in fast time-varying channels. In: *2006 14th European signal processing conference*, Florence, 4–8 September 2006. New York: IEEE.

23. Hrycak T and Matz G. Low-complexity time-domain ICI equalization for OFDM communications over rapidly varying channels. In: *40th Asilomar conference on signals, systems and computers (ACSSC '06)*, Pacific Grove, CA, 29 October–1 November 2006, pp.1767–1771. New York: IEEE.
24. Kun F, Leus G and Rugini L. CTH03-4: Alamouti space-time coded OFDM systems in time- and frequency-selective channels. In: *Global telecommunications conference (GLOBECOM '06)*, San Francisco, CA, 27 November–1 December 2006, pp.1–5. New York: IEEE.
25. Golub GH and Van Loan CF. *Matrix computations*. Baltimore, MD: Johns Hopkins University Press, 1996.
26. Taubock G, Hampejs M, Matz G, et al. LSQR-based ICI equalization for multicarrier communications in strongly dispersive and highly mobile environments. In: *IEEE 8th workshop on signal processing advances in wireless communications (SPAWC 2007)*, Helsinki, 17–20 June 2007, pp.1–5. New York: IEEE.
27. Hrycak T, Das S, Matz G, et al. Low complexity equalization for doubly selective channels modeled by a basis expansion. *IEEE T Signal Proces* 2010; 58: 5706–5719.
28. Hua H and Le-nan W. Low complexity LSQR-based block decision feedback equalizer for OFDM systems over rapidly time-varying channels. In: *2010 international conference on communications and mobile computing (CMC)*, Shenzhen, China, 12–14 April 2010, pp.438–441. New York: IEEE.
29. Taubock G, Hampejs M, Svac P, et al. Low-complexity ICI/ISI equalization in doubly dispersive multicarrier systems using a decision-feedback LSQR algorithm. *IEEE T Signal Proces* 2011; 59: 2432–2436.
30. Fong DC-L and Saunders MA. LSMR: an iterative algorithm for sparse least-squares problems. *SIAM J Sci Comp* 2011; 33: 2950–2971.
31. Paige CC and Saunders MA. Solution of sparse indefinite systems of linear equations. *SIAM J Numer Anal* 1975; 12: 617–629.
32. Golub G and Kahan W. Calculating the singular values and pseudo-inverse of a matrix. *J Soc Indus Appl Math, Series B: Numer Anal* 1965; 2: 205–224.
33. Toker C, Lambotharan S, Chambers JA, et al. Closed-loop quasi-orthogonal STBCs and their performance in multipath fading environments and when combined with turbo codes. *IEEE T Wirel Commun* 2004; 3: 1890–1896.
34. Schniter P. Low-complexity equalization of OFDM in doubly selective channels. *IEEE T Signal Proces* 2004; 52: 1002–1011.
35. Ahmed S, Sellathurai M and Chambers JA. Low complexity iterative method of equalization for OFDM in doubly selective channels. In: *Conference record of the 39th Asilomar conference on signals, systems and computers*, Pacific Grove, CA, 2005, pp.687–691. IEEE.
36. Rugini L and Banelli P. Performance analysis of banded equalizers for OFDM systems in time-varying channels. In: *IEEE 8th workshop on signal processing advances in wireless communications (SPAWC 2007)*, Helsinki, 2007, pp.1–5. IEEE.
37. Yang-Seok C, Voltz P and Cassara FA. On channel estimation and detection for multicarrier signals in fast and selective Rayleigh fading channels. *IEEE T Commun* 2001; 49: 1375–1387.
38. Attar H, Stankovic L, Alhihi M, et al. Deterministic network coding over long term evaluation advance communication system. In: *4th international conference on digital information and communication technology and its applications (DICTAP 2014)*, Bangkok, Thailand, 6–8 May 2014, pp.56–61. New York: IEEE.
39. Attar H, Stankovic L and Stankovic V. Cooperative network-coding system for wireless sensor networks. *IET Commun* 2012; 6(3): 344–352.
40. Nazir S, Stankovic V, Attar H, et al. Relay-assisted rateless layered multiple description video delivery. *IEEE J Selected Areas Commun* 2013; 31(8): 1629–1637.
41. Attar H, Alhihi M, Zhao B, et al. Network coding hard and soft decision behavior over the physical payer using PUMTC. In: *Proceedings of 2018 international conference on advances in computing and communication engineering (ICACCE 2018)*, Paris, 22–23 June 2018, pp.471–474. New York: IEEE.